JOURNAL OF AIRCRAFT
Vol. 34, No. 1, January–February 1997

Icing Calculations on a Typical Commercial Jet Engine Inlet Nacelle

Kamel M. Al-Khalil*
Cox & Company, Inc., New York, New York 10014
and
Theo G. Keith Jr.† and Kenneth J. De Witt‡
University of Toledo, Toledo, Ohio 43606

A procedure is presented to analyze a commercial jet engine inlet during icing. The essential steps in the numerical simulation are discussed: flowfield calculations, determination of droplet trajectories hitting the surface, and computation of the heat transfer phenomena. A three-dimensional flowfield solver utilizing the panel method was found to be adequate for modeling noncomplicated engine inlet nacelles at subsonic speeds. Droplet trajectories were produced using a three-dimensional grid-based code. Predicted collection efficiencies were in good agreement with experimental results. Heat transfer calculations are performed with the NASA Lewis ANTICE code. Two example cases are presented.

Nomenclature

AOA = angle of attack of body with the freestream air, deg
LWC = liquid water content in the freestream, g/m^3
MVD = mean volume droplet diameter in cloud, μm
m^o = surface runback mass flow rate, kg/m s
q_{surf} = surface heat flux, W/in.^{2}
S = surface distance from stagnation, positive inboard, m
T_s = skin temperature, °C
T_∞ = freestream static temperature, °C
V_∞ = freestream air velocity, m/s
β = droplet collection efficiency
θ = circumferential angle from the vertical about the inlet center axis, deg

I. Introduction

AIRCRAFT surfaces and engine inlets are subject to ice accumulation while flying through a cloud of supercooled liquid water droplets. Ice formation generally occurs on leading-edge surfaces and detrimentally affects the aircraft performance. In cases where the ice accretes on lifting surfaces, such as wings and horizontal tails, aerodynamic performance degradation occurs as a result of decrease in lift, increase in drag and stalling speed, and reduced stability and controllability of the aircraft. Although the problem is limited to subsonic speeds, supersonic jets are also exposed to the hazardous effects of icing during low-speed maneuvers such as takeoff/climb, descend/landing, and hold stages.

The mathematical and computational procedure involved in the simulation of aircraft icing encompasses several steps. First, the surface geometry of the aircraft components must be modeled and may be represented with many discrete grid points or surfaces (panels). Second, the air flowfield must be calculated at and about the body surface. Third, the liquid water droplet trajectories must be computed to determine the location and rate of impingement on the surface. Finally, a thermodynamic analysis must be performed on the surface water and the aircraft structure.

Only a few studies dealing with ice accretion on three-dimensional engine inlets are available in the literature. Among these studies is the work performed by Kim,[1] where a computational particle trajectory on a three-dimensional engine inlet was analyzed. The flowfield was obtained using a compressible three-dimensional full potential flow code. Also, Schuster[2] presented a computational scheme for obtaining droplet impingements on complex inlet geometries. However, since the flowfield was obtained using a Navier–Stokes (N–S) solver, the flow calculation required a much larger CPU time than if computed with a potential flow solver as in the present work. Ice accretion calculations on unprotected surfaces were recently performed by Bidwell.[3]

In the current study, the procedure for anti-icing calculations on a scaled Boeing 737-300 engine inlet model will be demonstrated. The anti-icing system simulated in the code can be either a hot compressor bleed air type, or an electrothermal type.[4–7] The engine nacelle is modeled as a number of quadrilateral panels. The flowfield calculations, at and about the inlet surface, were performed using the VSAERO panel code,[8,9] a three-dimensional potential flow solver. The code corrects for compressibility effects and has a module for boundary-layer calculations. The velocity is calculated at each grid point on a three-dimensional grid system specified by the user, and is written to an output file that will subsequently be used in the water droplet trajectory calculations.

Each water droplet in the atmosphere is subject to drag, buoyancy, and gravity forces, depending on its size. The droplet's trajectory intersects the potential flow streamlines as the droplet approaches the inlet surface. Integration of the droplet trajectory equation is performed using the velocities interpolated from the grid-based system. Trajectories were calculated using the ICE code.[10] Comparisons will be made between the ICE code results on the inlet model and experimental data obtained on the same scaled model at the NASA Lewis Icing Research Tunnel by Papadakis et al.[11]

The final step in the numerical simulation is to model the heat transfer on the engine nacelle and the impinging water that flows downstream on the surface. The computer code ANTICE for simulation of running wet and evaporative anti-icing systems was developed for this purpose.[4,6] Both air and elec-

Presented as Paper 94-0610 at the AIAA 32nd Aerospace Sciences Meeting, Reno, NV, Jan. 10–13, 1994; received Feb. 13, 1994; revision received Sept. 17, 1996; accepted for publication Nov. 12, 1996. Copyright © 1996 by the American Institute of Aeronautics and Astronautics, Inc. All rights reserved.

*Engineering Scientist. Member AIAA.
†Professor, Mechanical Engineering Department. Associate Fellow AIAA.
‡Professor, Chemical Engineering Department. Member AIAA.

trothermal systems are modeled, and two example cases are illustrated: 1) climb and 2) descent.

II. Flowfield Computation

There exist several numerical solvers for predicting flowfields. These differ in the technique used to solve the prevailing governing equations and the associated assumptions. Although thought to yield the most accurate results, full N–S solvers tend to require large amounts of time and memory allocation when run on a digital computer. The next best alternative is to solve the compressible Euler equations (nonviscous version of the N–S equations). Although the computational effort in the numerical solution of the latter equations is more reasonable than in the case of the N–S equations, additional assumptions may be made to reduce the computational overhead greatly and still maintain reasonable accuracy for subsonic flows. This is accomplished by solving the potential flow equations in which it is assumed that the fluid, air in this case, is inviscid and the flow is irrotational.

VSAERO computes the nonlinear aerodynamic characteristics of arbitrary configurations in subsonic flows.[8,9] Basically, it calculates the linearized potential flow external to a body or internal to a duct where the normal velocity on the surfaces bounding the flow is specified. Wakes are used to account for nonlinear effects of vortices, while viscous effects are treated in an iterative loop that couples the potential flow to a two-dimensional integral boundary-layer solver. Since the normal velocity to a wake surface is zero, wake panels are iteratively oriented with the local flow. Compressibility effects are accounted for by applying either the Karman–Tsien correction or the Prandtl–Glauert linearization.

VSAERO creates off-body velocity grid distributions that can be scanned on rectangular or cylindrical coordinates as specified by the user. Subsequently, the droplet trajectory code, ICE, computes the local freestream velocity by interpolation from the grid system to solve the water droplet momentum equations. Geometric and aerodynamic results were examined using the interactive graphics package OMNI3D, which is tailored for postprocessing VSAERO and ICE solutions.

III. Droplet Trajectory Calculations

Calculation of accurate droplet impingements on the surface is a crucial step in the design of ice-protection systems. The impingement limits on the surface may be the only elements of interest in some cases where predicting the direct impingement regions is what determines which areas need to be protected.

Droplet trajectory information is obtained by integrating the equation of motion of individual droplets. Three basic assumptions are generally made: 1) water droplets do not interact with each other, 2) the flowfield is assumed to be undisturbed by the droplets, and 3) the shape of each droplet is spherical. The last assumption is necessary to predict the drag force imparted on the droplet because of the effect of the local relative air velocity.

Atmospheric conditions that may pose potential hazards for an airplane have been defined by the Federal Aviation Administration (FAA) in a form of graphical charts referred to as icing envelopes.[12]

The procedure used in the ICE code is to compute the rate of water catch on a particular panel by iteratively predicting the starting location of four upstream particles whose trajectories would coincide with the corresponding four panel corners. To represent quantitatively the rate of water impinging on the surface, the standard collection efficiency parameter β is used. The relative speed of droplets far upstream of the surface is equivalent to the flight speed. Therefore, the rate of water flux approaching the surface far upstream is the product of LWC and V_∞.

As a droplet approaches the airplane surface, the effect of drag and gravity will alter its initial straight path. Thus, the rate of water flux striking the surface becomes [β LWC V_∞], where β is referred to as the local collection efficiency ($\beta < 1$). Therefore, the value of β on a particular panel is the ratio of the panel area to the area formed far upstream, and normal to the local airflow, by the rectangular stream tube that is outlined by the four trajectories hitting the panel corners.

Validation of the ICE code was done primarily with experimental data on two-dimensional airfoil shapes, and with numerical results from other codes for two- and three-dimensional geometries. In the current study, comparisons will be made with experimental data from a scaled Boeing 737-300 engine inlet model obtained during tests conducted at the NASA Lewis Icing Research Tunnel by Papadakis et al.[11]

IV. Thermodynamic Analysis

The analytical thermodynamic model has been described in earlier studies.[6,7] The various modes of heat transfer occurring within an anti-iced aircraft surface and the collected water, referred to as runback when it flows on the surface, have been accurately represented. The mathematical formulation is based on a two-dimensional steady-state heat transfer model along a surface streamline. The structure may be represented by a number of composite layers. Any one layer can be composed of several heater zones, each with a specified power density.

Anti-icing of the surface may also be accomplished using a hot air system. This is currently modeled such that hot air of given mass flow rate and temperature is supplied to the inner surface in the vicinity of the stagnation line, and flows back into the cowl in the direction of surface streamlines. A user can also specify a distribution of variable heat flux at the surface to obtain an approximate system behavior as a first step in the design and/or analysis process (i.e., evaporative, running wet, or freezing runback).

Also modeled is the runback flow behavior on the surface: continuous surface coverage at the direct impingement regions, vs rivulet structure flow downstream. Rivulets are individual narrow streams of water. A stability analysis was performed for the prediction of rivulets.[5,6]

V. Overall Computational Procedure

The following provides detailed computational steps followed during the icing simulation in the order they were performed.

A. Flowfield

The nacelle geometry was represented by a discrete number of quadrilateral panels. The flow on and about the nacelle was assumed to be undisturbed by nearby objects such as the pylon and wing or tail surfaces. It is good practice to have a more dense panel distribution at locations of high curvature and the leading-edge surfaces where water droplets are expected to impinge.

Aside from specifying the freestream velocity vector, wakes must be attached to the body at separation lines on panels. In this case, initial wake lines are defined to separate the jet exhaust from the freestream on the rear end of the nacelle. Also, sets of nonzero velocity panels are identified, and, they correspond to panels representing the fan face and panels representing the jet exhaust. The velocity on each of these sets of panels is specified. For the fan face, this can be roughly estimated from the known mass flow rate of freestream air ingested by the engine using the one-dimensional compressible gasdynamics relations and area ratios. For the case of the exhaust gas, it depends on the combustion process and several other factors that were found to have little effect on the flow near the nacelle leading edge, the region of interest to icing.

Since icing calculations are to be performed at several circumferential locations (θ locations), surface streamlines must

be calculated at those regions. It is assumed, and substantiated in icing tunnel tests, that runback water flows on the surface to downstream regions as a result of aerodynamic shear forces following streamline paths. Thus, a number of streamlines are computed on the surface along which aerodynamic variables are calculated. These include pressure and friction coefficients. Also, it is along those streamlines that droplet impingement efficiencies are calculated for the corresponding surface panels crossed by the streamlines.

For each surface streamline, an off-body velocity scan is defined such that the droplets, which may hit the surface along a particular streamline, travel within the boundaries of that velocity scan. VSAERO allows a multiple number of velocity scans to be generated in either a rectangular or cylindrical coordinate system. The latter was chosen since it was thought to be more appropriate for engine inlet geometries that are nearly axisymmetric.

A droplet path is disturbed only when it approaches the surface of the aircraft where the air velocity gradients are large. Therefore, a coarse mesh of off-body velocity scan was used for interpolation of the local freestream velocity when the droplet is still far from the surface. Near the surface, however, a fine mesh for air velocities was generated for the purpose of obtaining more accurate results where the relative velocity vector changes rapidly.

B. Droplet Trajectories

Once a flowfield solution was obtained, droplet trajectories were calculated on panels that crossed the surface streamline considered in the analysis. The ICE code reads flowfield data from the binary graphics file generated by VSAERO. An input file specific to the ICE code is set up in which some parameters are defined along with surface streamlines or panels for which the collection efficiency is desired.

The code starts from the initial droplet release location. Integration of the droplet equation of motion using the air velocity interpolated from the grid yields a trajectory for a droplet that appears very much like an off-body streamline. In practice, a mean volume droplet diameter of 16–20 μm has been very commonly used for design, analysis, and testing purposes. For such a size, it was found that an initial release location may be assumed to be along an off-body streamline that passes close to the panel of interest, or more precisely, near the stagnation point corresponding to an on-body streamline of interest.

The latter information also can assist the user in defining the size and extent of an off-body velocity grid scan. Practically, the grid scan volume is made large enough to contain at least the trajectories. This was done so that if the target location is missed, an extrapolation scheme could be used to obtain a new guess for the location of the droplet release point until convergence on a specified panel corner is reached within a user specified tolerance.

C. Thermodynamics

ANTICE is used to simulate the heat transfer characteristics at the surface as described in Sec. IV. Before the code is executed, the following information must be available: 1) surface pressure coefficient distribution along a streamline; 2) distance between two adjacent surface streamlines representing a zone of interest in the analysis, this is an option for three-dimensional flows such as on swept wings or inlet nacelles; and 3) collection efficiency distribution at the surface.

Details on the numerical procedure are presented in Ref. 6.

VI. Examples and Discussion

Two example cases, climb and descent, will be considered to demonstrate the calculation procedure. In these examples, the model considered is a 0.2547-scaled version of the Boeing 737-300 engine inlet nacelle. This was chosen because of the availability of experimental data[11] for comparison purposes. The test conditions considered are illustrated in Table 1.

Following the procedure described earlier, the flowfield on and about the nacelle was obtained. When examining the results, it should be noted that the difference between the climb and descent cases are the angle of attack and the amount or ram air ingested by the engine. Surface streamlines were generated at several θ locations along the nacelle perimeter. These are shown for the climb and descent conditions in Figs. 1 and 2, respectively. As expected, the streamlines along the sides of the nacelle tend to go upward in the descent case as a result of the high AOA.

Surface pressure coefficients are illustrated in Figs. 3 and 4 at θ = 45 and 135 deg for the climb case, respectively. Reference 13 illustrates flowfield, trajectory, and anti-icing results at additional θ locations. The corresponding results for the descent case are shown in Figs. 5 and 6, respectively. The general trend seen is that the pressure coefficient on inboard surface of the nacelle is larger than it is on the outer surface. This is directly related to the amount of air ingested by the engine.

Table 1 Test conditions of two example cases

Variable	Climb	Descent
AOA, deg	0	15
Inlet airflow, kg/s	7.8	5.2
V_∞, m/s	77.2	76.1
T_∞, °C	−17.78	−17.78
LWC, g/m^3	0.25	0.35
MVD, μm	20.36	16.45

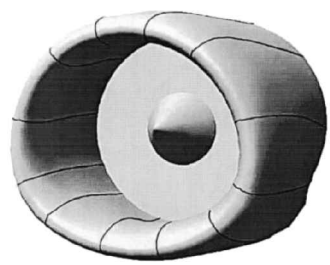

Fig. 1 Surface streamlines (climb).

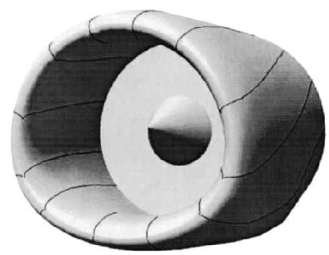

Fig. 2 Surface streamlines (descent).

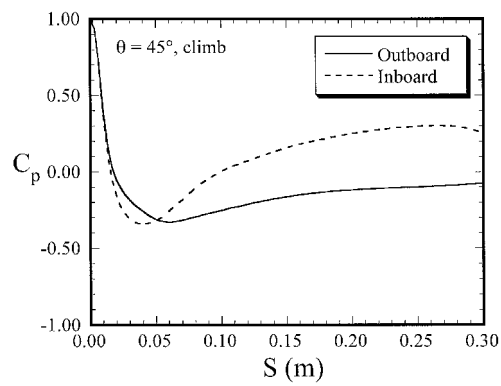

Fig. 3 Pressure coefficient.

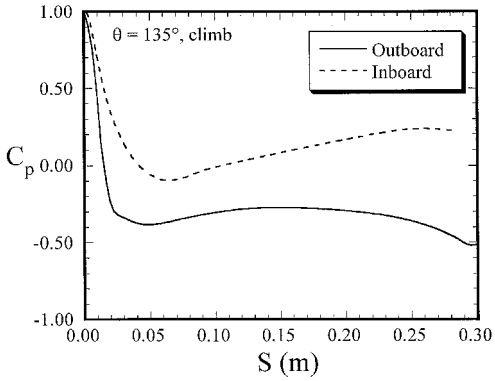

Fig. 4 Pressure coefficient.

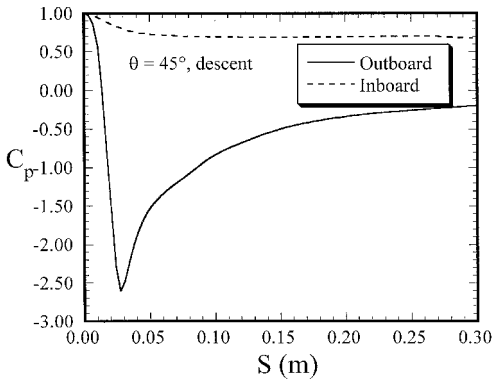

Fig. 5 Pressure coefficient.

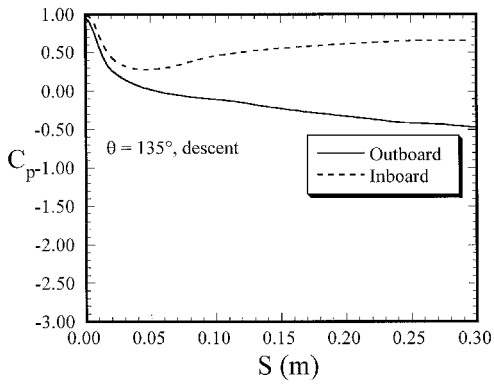

Fig. 6 Pressure coefficient.

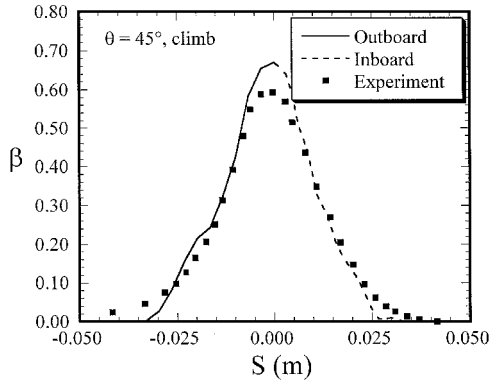

Fig. 7 Collection efficiency.

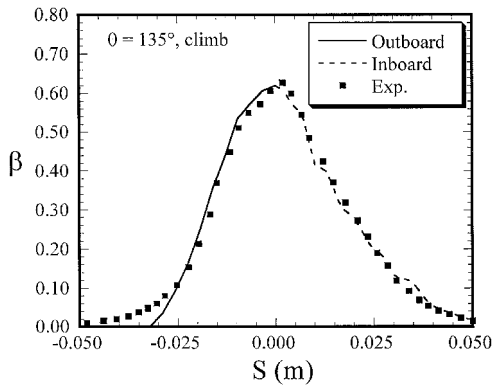

Fig. 8 Collection efficiency.

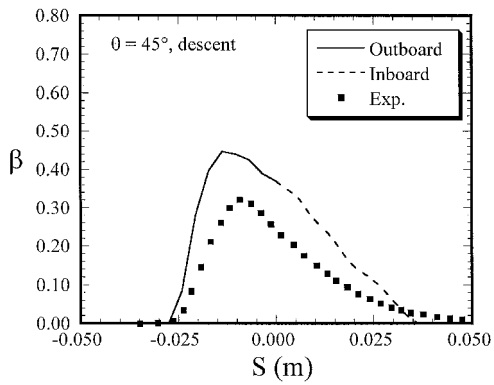

Fig. 9 Collection efficiency.

This phenomenon is rather clear in the descent case where the engine is running at a low power and causing a large deceleration of the inboard air.

The spikes observed in the C_p curves of the descent case at θ = 45 deg (Fig. 5) are caused by the rapid acceleration and deceleration of the air from the stagnation line that exists on the inboard surface at the upper lip as the air flows around the highlite. As a result of this behavior, separation of the boundary layer was found to occur on the outboard surface at the location of adverse pressure gradients. The plots shown are distributions along surface streamlines that start at, but may not remain on, a specified angle θ. Therefore, consistency must be maintained if a comparison is to be made with results of other computer codes or experimental data. The accuracy and verification of the commercial computer program VSAERO has been addressed in the literature.[8,9]

The next step in the calculation process was to obtain droplet collection efficiency distributions along the surface streamlines. The procedure described earlier was carried out at θ = 45 and 135 deg. The corresponding collection efficiency distributions are shown in Figs. 7 and 8 for the climb case, and in Figs. 9 and 10 for the descent case, respectively. Close agreement was obtained between the experimental and numerical results for climb case, despite an experimental repeatability of ±10% from the mean[11] between test runs for a given test condition. The correlation for the descent case was not as good. The source of discrepancy may be associated with the high AOA in the descent case and that potential flow solvers are incapable of accurately modeling the flow separations and vortices associated with viscous fluids behavior. Additionally, the band of test repeatability (±10%) in those cases was a little wider than the difference between the predicted and the measured parameters.

A comparison between the current numerical results and those presented in Ref. 11 showed a similar trend in the deviation from the experimental results. Nonetheless, the results may be considered acceptable from an engineering point of view, despite the large number of variables affecting the nu-

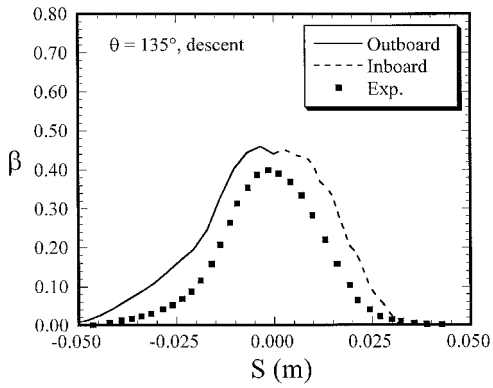

Fig. 10 Collection efficiency.

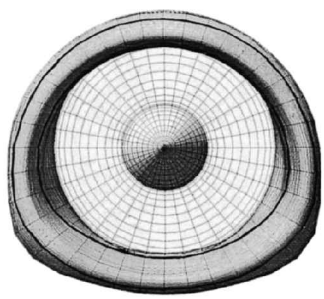

Fig. 11 Impingement limits (climb).

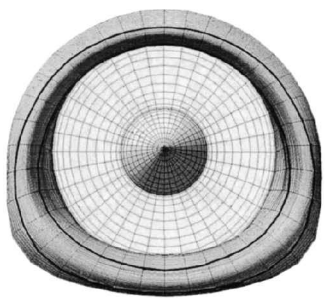

Fig. 12 Impingement limits (descent).

merical as well as the experimental results. The ICE code had also been verified earlier with other geometries (a cylinder, a sphere, and a NACA 0012 airfoil geometries).[10] The trend showed good agreement with experimental results. An excellent agreement was obtained when comparing to analytical results of droplets impingement on cylinders and spheres.

The impingement limits were not captured closely, because in the actual test setup, at the NASA Lewis Icing Research Tunnel (IRT), the water droplet atomizing system cannot produce a constant drop size, but rather a distribution. This is true at least in the range of droplets considered in this study (16–20 μm). The actual distribution would include a small percentage of droplets larger than the mean. Large droplets are known to impinge further downstream on the surface because of their higher momentum. The numerical calculations assumed a uniform droplet size rather than a distribution. Also, a phenomenon that is generally observed in the IRT is the formation of a secondary ice impingement, known as feather ice growth.[14] This occurs just beyond the initial impingement limits because of the existence of nucleation sites that then become targets for direct impingement.

Numerical prediction of impingement limits that are associated with very small values of β becomes tedious and CPU intensive. This is because the droplet trajectories at these locations are almost parallel to the surface just before hitting or missing the body (this is especially true for large drops). It is the larger droplets that determine the impingement limits because of their higher momentum and tendency to follow more nearly straight paths than smaller droplets. Impingement limits calculated with the ICE code are depicted in Figs. 11 and 12 by the dark lines near the leading edge for climb and descent cases, respectively. The effect of the AOA is very clearly shown, despite the difference in the inlet air mass flow rate in these two cases.

The computer code used in Ref. 11 to obtain the flowfield solves the full partial differential equations of compressible transonic potential flow with the finite difference method. That method is well known to be more CPU time consuming than panel codes such as VSAERO. This indicates that, for such a problem and for subsonic airflows, a panel technique may be sufficient to obtain reliable flow solutions.

The last step in the analysis was to predict the heat transfer phenomena using the ANTICE code. For such a three-dimensional model, the stagnation line seldom occurs at the nacelle highlite. This requires accurate prediction of water impingement regions for the design of an anti-icing system as well as the decision on the extent of the area that need to be protected. The following parameters affect the anti-icing system performance: inlet air mass flow rate, freestream velocity, angle of attack, droplet size, ambient temperature, and liquid water content as shown in Table 1.

The anti-icing system was assumed to be an electrothermal type. The heaters are rated at 15 W/in.^{2} and extend 5 cm on each side of the stagnation line around the nacelle perimeter. The latter assumption may not be the practical design approach. Its purpose is to demonstrate the need to analyze precisely many sections of the inlet caused by the three-dimensional effects to establish a properly designed ice-protection system.

The skin temperature and the surface runback mass flowrate distributions are shown in Figs. 13 and 14 at the circumferential locations θ = 45 and 135 deg, respectively, for the climb

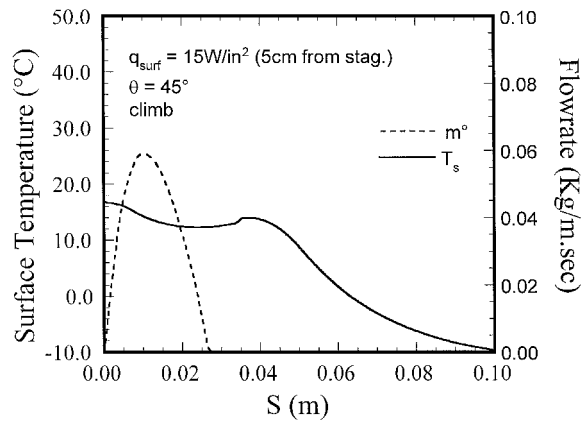

Fig. 13 Anti-icing results.

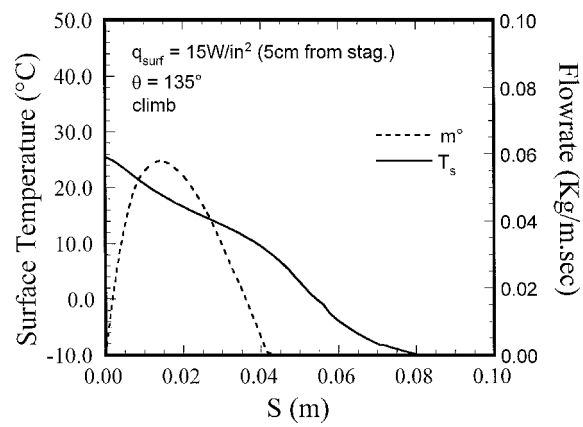

Fig. 14 Anti-icing results.

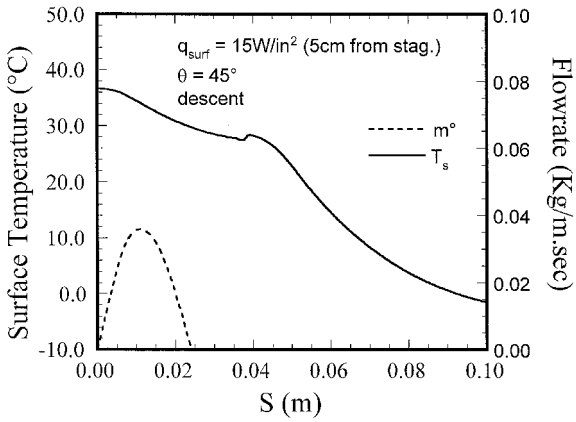

Fig. 15 Anti-icing results.

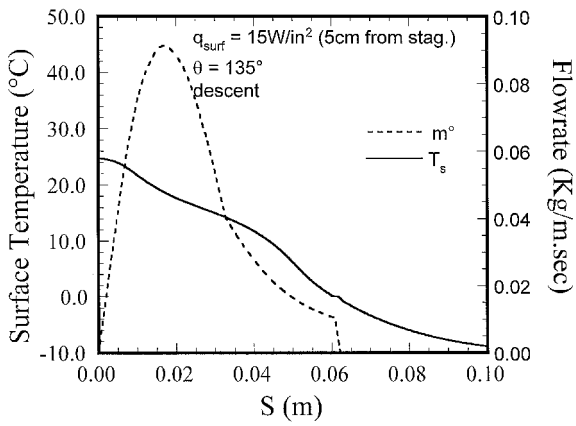

Fig. 16 Anti-icing results.

case. The corresponding plots for the descent case are shown in Figs. 15 and 16. The engine's operation and safety is mainly affected by the freezing runback on the nacelle's inboard surface. Thus, the variables in those figures were plotted against the distance from the stagnation point along inboard streamlines only.

In all cases, liquid water exists on the surface within the direct impingement regions. The code also predicted that the runback water would be totally evaporated before reaching the unprotected regions ($S > 0.05$ m) with the exception of one case. That is at $\theta = 135$ deg for the descent case, as depicted in Fig. 16, where the water began to freeze at $s = 0.062$ m.

The increased amount of water impinging on the surface in the latter case not only increased the runback mass flow rate, but also kept the water temperature relatively low. This reduced its potential to evaporate. The runback water temperature was reduced as water approached the boundaries of the heated region such that evaporation was diminished even further. This trend continued beyond those boundaries and the runback water temperature continued to decrease until it reached the freezing point. At that location, the remaining liquid water froze. The amount of ice buildup becomes a function of exposure time to the icing conditions.

Despite providing equal amounts of heating to the surface in all of the previous cases, it is clear that the performance varies from one location to another because of variations in the local impingement and aerodynamic properties. The latter also depends on the model geometry and the AOA.

The accuracy of the ANTICE code predictions have not been verified in the current study because of lack of experimental data for the configuration considered. However, comparisons with test results on a NACA 0012 airfoil in the NASA IRT were presented in an earlier study[7] and a good general agreement was obtained. The sources of differences were attributed to nonuniformity of the surface heat flux, and the surface roughness assumed by the user to predict the heat transfer coefficients. This mostly affected the predictions of surface temperature that could be off by 10°C. However, the system performance prediction was correct in all cases considered, i.e., the existence of frozen runback on the surface vs a clean leading edge.

VII. Conclusions

A procedure was presented to analyze a commercial jet engine inlet icing process for subsonic flight speeds. The essential steps in the numerical simulation were thoroughly discussed. These may be listed as follows: flowfield calculations, determination of droplet trajectories, and computation of the heat transfer phenomena.

A flowfield solver utilizing the panel method was found to be adequate for modeling noncomplicated engine inlet geometries at subsonic speeds. Consequently, it should be suitable for other components such as wings as long as the surface is free of ice. A major advantage of potential flow solvers, especially the panel method type, is the impressive computational speeds. Of course, the results may not be necessarily adequate for assessing aerodynamic performance properties such as lift and drag. This is especially true at high AOA when ice has already accreted on the leading edge causing spanwise vortex flow from a swept wing's root.

The droplet trajectories produced by the ICE code were in good agreement with experimental results at zero degrees AOA. The agreement was acceptable for flows at the large AOA. This behavior may be attributed to the breakdown of potential flow solvers at high AOA and the uncertainty in the experimental data as a result of the large number of variables involved in the process.

The relative variations predicted in the anti-icing system performance around the nacelle perimeter, despite providing equal amounts of heating, proves the need for such a simulation tool for accurate analysis and design. Consequently, the design of an anti-icing system is not a simple procedure. The component being protected must be accurately modeled in all aspects of the analysis. Environmental conditions that may cause icing problems to the engine must be taken into consideration in the simulation and design stages.

Acknowledgments

The present investigation was sponsored by the Icing and Cryogenic Technology Branch of the Propulsion Systems Division at NASA Lewis Research Center, Cleveland, Ohio. This support is appreciated by the authors.

References

[1]Kim, J. J., "Computational Particle Trajectory Analysis on a 3-Dimensional Engine Inlet," AIAA Paper 85-0411, Jan. 1985.

[2]Schuster, E. P., Gambill, J. M., and Fisher, M. S., "Computational Icing Analysis of Aircraft Inlets," AIAA Paper 92-3178, July 1992.

[3]Bidwell, C. S., "Ice Accretion Prediction for a Typical Commercial Transport Aircraft," AIAA Paper 93-0174, Jan. 1993.

[4]Al-Khalil, K. M., Keith, T. G., De Witt, K. J., Nathman, J. K., and Dietrich, D. A., "Thermal Analysis of Engine Inlet Anti-Icing Systems," AIAA Paper 89-0759, Jan. 1989.

[5]Al-Khalil, K. M., Keith, T. G., and De Witt, K. J., "Further Development of an Anti-Icing Runback Model," AIAA Paper 91-0266, Jan. 1991.

[6]Al-Khalil, K. M., Keith, T. G., and De Witt, K. J., "Development of an Improved Model for Runback Water on Aircraft Surfaces," AIAA Paper 92-0042, Jan. 1992.

[7]Al-Khalil, K. M., and Potapczuk, M. G., "Numerical Modeling of Anti-Icing Systems and Comparison to Test Results on a NACA 0012 Airfoil," AIAA Paper 93-0170, Jan. 1993.

[8]Maskew, B., "Prediction of Subsonic Aerodynamic Characteristics: A Case for Low-Order Panel Methods," *Journal of Aircraft*, Vol. 19, No. 2, 1982, pp. 157–163.

[9]"VSAERO User's Manual," Analytical Methods, Inc., Redmond,

WA, June 1991.
[10]Nathman, J. K., ''Particle Trajectory and Ice Accretion Modules for Program VSAERO,'' Analytical Methods, Inc., Redmond, WA, Rept. 8805, July 1988.
[11]Papadakis, M., Elangonan, R., Freund, G. A., Jr., Breer, M., Zumwalt, G. W., and Whitmer, L., ''An Experimental Method for Measuring Water Droplet Impingement Efficiency on Two- and Three-Dimensional Bodies,'' NASA CR-4257, Nov. 1989.
[12]''Transport Category Airplanes,'' Federal Aviation Regulations, Airworthiness Standards, Pt. 25, Appendix C, FAA, Washington, DC, 1982.
[13]Al-Khalil, K. M., Keith, T. G., and De Witt, K. J., ''Icing Calculations on a Typical Commercial Jet Engine Inlet Nacelle,'' AIAA Paper 94-0610, Jan. 1994.
[14]Reehorst, A. L., Ratvaski, T. P., and Sims, J., ''Close-Up Analysis of Inflight Ice Accretion,'' AIAA Paper 94-0804, Jan. 1994.